Appl. Phys. B 61, 319–323 (1995)

Applied Physics B Lasers and Optics

Efficient vacuum-ultraviolet generation by anti-Stokes Raman scattering using a cryogenic Raman cell

H. Moriwaki[1], A. Nakamura[1], S. Wada[2], H. Tashiro[2]

[1] Department of Applied Physics, Science University of Tokyo, 1-3 Kagurazaka, Shinjuku-ku, Tokyo 162, Japan
[2] The Institute of Physical and Chemical Research (RIKEN), 2-1 Hirosawa, Wako-Shi, Saitama 351-01, Japan
(FAX: + 81-3/3260-4772)

Received: 25 April 1995 / Accepted: 9 June 1995

Abstract. We have investigated the increase of efficiency for high-order anti-Stokes Raman scattering using a cryogenic Raman cell. By cooling the cell to liquid-nitrogen temperature, output energies of the 9th-order anti-Stokes wave at 133 nm in normal hydrogen were enhanced by a factor of 10, and the 11th-order anti-Stokes line at 141 nm in normal deuterium appeared, while no output was observed at room temperature. No output energy enhancement, however, was obtained using cooled para-hydrogen as a result of multiple rotational Raman scattering. For long-term operation, the output window surface of the Raman cell was kept at above 200 K in order to protect it from deposition, the absorption of which is detrimental to VUV transmission.

PACS: 42.65; 42.55; 07.60; 07.20

In wavelength conversion by stimulated Raman scattering, cooling of the Raman medium is a common effective technique to improve the scattering efficiency. Especially in a rotational Raman converter, such as the para-hydrogen Raman laser at 16 μm [1–3], the increase of the Raman gain coefficient is known to be remarkable. For high-order Anti-Stokes (AS) Raman scattering, which has also become an efficient method for VUV generation [4–11], cooling will contribute to increase the scattering efficiency. In contrast to the complicated design of a para-hydrogen Raman cell with multiple-pass structure [3], the cooling device of a VUV Raman cell seems to be much simpler. So far, two types of straight-pass Raman cells have been used with liquid nitrogen, but their performances are still far from being satisfactory. One was designed to cool only the central portion of the cell, and the entrance window was blown with dry nitrogen to prevent water-vapor condensation [4]. Even with this simple design, it functioned for a certain period but suffered from pointing instability of the beam due to gas convection. The other one was set up in a concentric configuration of three cylinders with vacuum insulation for liquid nitrogen. By cooling the whole cell, the VUV output was increased several times, but the improved output could not be sustained for a long time. It was pointed out that the contaminations observed on the window might cause serious reduction in the VUV transmission [11].

In this work, we developed a liquid-nitrogen-cooled Raman cell the windows of which were protected from deposition of contaminants. Using the cooled Raman cell, the VUV anti-Stokes radiation enhancement was studied in detail with normal hydrogen (n-H_2), and also with normal deuterium (n-D_2) and para-hydrogen (p-H_2).

1 Design of the cryogenic Raman cell

A schematic diagram of the liquid-nitrogen-cooled Raman cell is presented in Fig. 1 together with the VUV monitoring system. The Raman cell has a threefold concentric-cylinder structure. The inner hydrogen cell is made of a stainless steel tube 90 cm in length and 4 cm in diameter. The characteristic feature of the cell is the heating of the exit window by an electric heater which is coiled and fixed to the window with a ceramic adhesive. The 10 cm long stem between the heater and the coolant reservoir produces a temperature gradient to minimize heat conduction and to achieve optical homogeneity in the gas medium.

The input and output windows are made of SiO_2 and MgF_2, respectively, and are sealed with a spring-coil O-ring coated with indium (Helicoflex HN-100). The temperature of the output window is monitored with a copper–constantan thermocouple attached onto its edge. The Raman cell, which is directly connected to the VUV separator, is placed in a vacuum tube 10 cm in diameter. The vacuum tube and the wavelength separator are evacuated to a pressure of about 2×10^{-5} Torr using a turbomolecular pump.

The temperature of the Raman-active gas was not directly measured but estimated from the pressure monitored with a vacuum gauge using the ideal gas

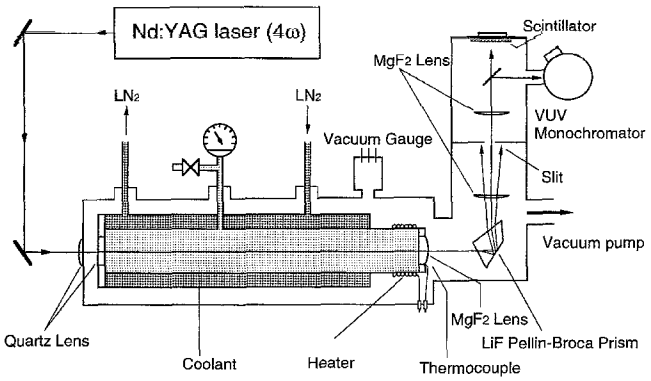

Fig. 1. Schematic of the liquid-nitrogen-cooled Raman cell and the monitoring system

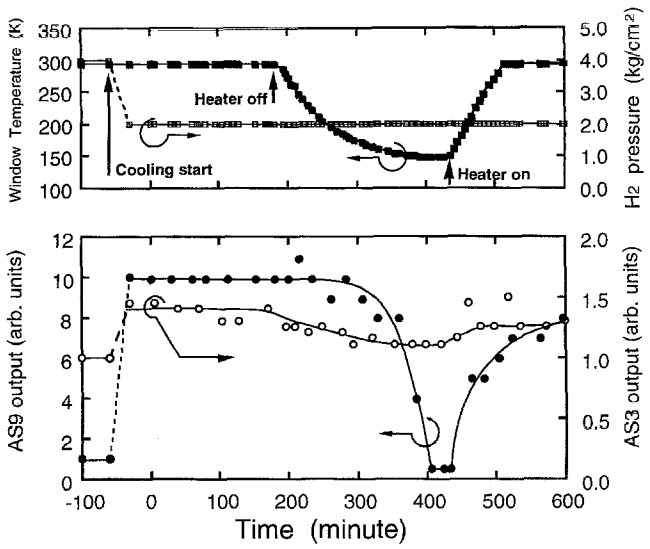

Fig. 2. Time course of temperature change of gas (*upper*) and window and output energy changes when the Raman cell cooling starts. Pulse energy variations of AS3 and AS9 pulses are shown, being normalized to energies before the start of cooling (*lower*)

equation. The estimation gave only approximate values because no correction for the non-uniformity of temperature in the gas container was carried out. Considering the volume that is surrounded by the liquid-nitrogen coolant, however, it is likely that the estimated values agree with the gas temperature at the center of the cell.

2 Experimental

Experimental procedures of VUV generation and characterization of output of the AS radiation have already been described in a previous paper [9]. A fourth-harmonic pulse from a Q-switched Nd: YAG laser (100 mJ, 8 ns) was focused into the cooled Raman cell using a quartz lens ($f = 600$ mm). The emitted beam was led directly to the wavelength separator with a LiF Pellin-Broca prism. The selected AS beam passing through the slit was divided into two beams by a LiF plate. One was introduced to a VUV monochromator (Minuteman 302-VM) and detected with a biplanar phototube (Hamamatsu R1193U-04) or with a solar-blind photomultiplier (Hamamatsu R972). The second beam was used to monitor the beam profile with a scintillator plate and a camera.

Pulse energies were measured with the following procedure. Radiation was introduced to the VUV monochromator after being scattered through a sand-blasted MgF_2 plate in order to minimize the influence of non-uniformity in the VUV beam patterns. Detection with the biplanar phototube (AS1–AS4) was calibrated to absolute energies of AS1–AS3 with a pyroelectric joulemeter (GenTec ED-200). Combining the data detected with a photomultiplier using the sensitivity curves of the detector, the calibration of anti-Stokes pulse energies was carried out assuming that the spectral response of the VUV monochromator is constant.

3 Results and discussion

It took about 30 min to fill the reservoir with liquid nitrogen, as shown in Fig. 2. During filling, the beam emitted from the Raman cell fluctuated and varied its position. It was confirmed, however, that within half an hour after the start of filling, the beam returned to the position that it occupied before cooling. Such beam stability guaranteed the ease of optical alignment as well as the minimum change of the optical path during temperature variation in the following experiment.

Figure 2 also shows the relation between output intensities and exit-window temperature. Pulse energies are plotted for AS3 and AS9. The record restarted at $t = 0$ when the cell was stabilized at liquid-nitrogen temperature. The vertical axis showing the output intensity is scaled relative to values before cooling. For the first 200 min during which the temperature of the exit window was kept at 293 K, VUV output appeared quite constant. The output intensity of AS9 was enhanced by one order of magnitude by cooling, while only a slight increase of 40% was observed for the output intensity of AS3. The heater was switched off at 180 min. Until the temperature dropped to 220 K at 220 min, VUV output did not change. The subsequent temperature drop of the window to 150 K, however, caused serious signal reduction of 90% at 400 min for AS9. On the other hand, for AS3, the energies were decreased slightly by 25% even at 420 min but cooling enhancement was still noticeable. At 430 min, the heater was switched on again, and the temperature of the window as well as the output signals of AS3 and AS9 began to increase immediately. The exit-window temperature returned to room temperature at 510 min. Energies of AS3 recovered to the level before switching off the heater but only a 70% recovery was obtained for AS9. This finding suggests that the contamination on the window surface was more detrimental to the VUV wave of AS9 than to the UV wave of AS3. The incomplete recovery obtained by raising the temperature does not imply permanent contaminant deposition on the surface but insufficient evacuation, because the transmission recovered fully once the whole cell was heated to room temperature. On the basis of these observations, we could

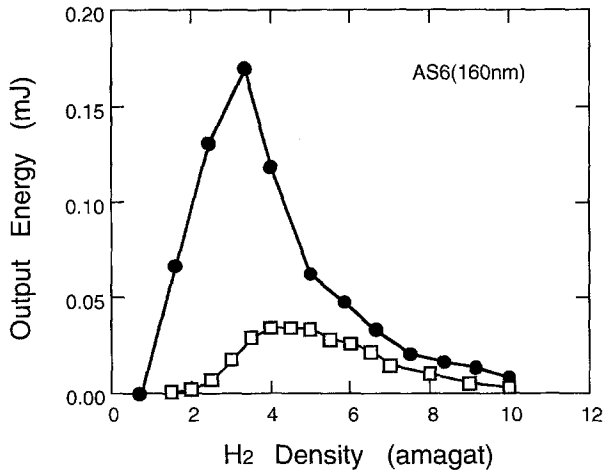

Fig. 3. Density dependence of the 6th-order AS wave in n-H_2 at 77 K (*filled circles*) and 293 K (*open squares*)

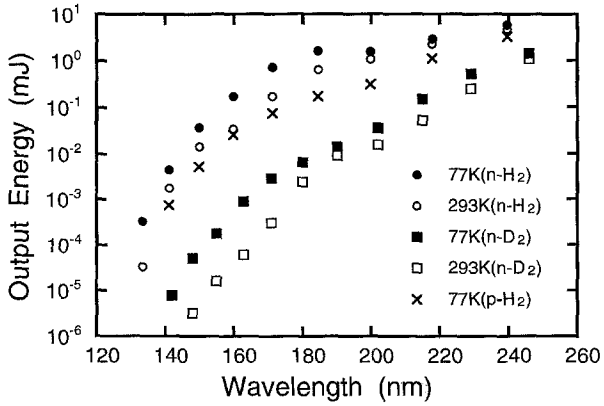

Fig. 5. Output pulse energies of individual AS waves. *Filled circles* and *squares* represent values for n-H_2 and n-D_2 at 77 K, respectively. *Open circles* and *squares* indicate values for n-H_2 and n-D_2 at room temperature, respectively. *Crosses* show energies of p-H_2 at 77 K

operate the cell for more than 10 h by keeping the window temperature at 250 K in the following experiments.

Figure 3 shows the dependence of output energies of AS6 on n-H_2 density at 77 K and 293 K. Filled circles represent energies averaged over 10 pulses of AS6 at 77 K, and open squares those at 293 K. Output energies were maximized at a density of 3.3 amagat, which was lower than the corresponding value at 293 K. In addition to the gain increase due to cooling, the change of the optimum density also affected the phase-matching condition, as shown in Fig. 4, where the beam profiles at optimum pressures for both temperatures are presented. The vertical scale of the intensity obtained directly from a photodensitometer was not linearized; thus, the qualitative changes were clearly observed. It is obvious that the profile at 77 K is narrower and the center component is more intense. A comparison of output energies at room and liquid-nitrogen temperatures is presented in Fig. 5. As expected from Fig. 3, enhancement effects became more pronounced for higher orders of anti-Stokes lines.

Table 1 also presents the gain of n-D_2 and p-H_2 for both room temperature and liquid-nitrogen temperature. The Raman line-widths at room and liquid-nitrogen temperatures are reported only for n-H_2. We used estimated values reported in [12–14] for p-H_2 and n-D_2. VUV output pulse characteristics obtained using these media are shown in Fig. 5. Absolute energies for both gases were small compared with those of n-H_2. The cooling-enhancement factors increased gradually for higher-order AS lines as in n-H_2. As for the factor itself, there is little difference between n-D_2 and n-H_2:

$$g_R = \frac{16\pi^2 c^2}{\eta_{-1}^2 \hbar \omega_{-1}^3} \frac{\Delta N}{\Delta \omega_R} \left(\frac{d\sigma}{d\Omega}\right), \tag{1}$$

where ΔN, ω_{-1}, η_{-1}, $\Delta\omega_R$, and $(d\sigma/d\Omega)$ are the population probability difference between the initial and final states of the Raman transition, the angular frequency of the first Stokes (S) wave, the refractive index at ω_{-1}, the Raman linewidth, and the differential cross section of Raman scattering, respectively. Considering temperature-dependent quantities, g_R obtained by cooling to 77 K is estimated to be 1.41 times of the value at 293 K, as shown in Table 1.

The AS Stimulated Raman Scattering (SRS) is a Raman-resonant four-wave-mixing process. Once the S1 field is created in SRS, AS1 generation starts by combination of the P and S1 waves. The AS2 field is produced by coupling of P, S1, and AS1 waves. In this manner, the ASn component is successively generated by the mixing of P, S1, and AS_{n-1}. In the simplest model with a plane-wave approximation under the phase-matching condition, the

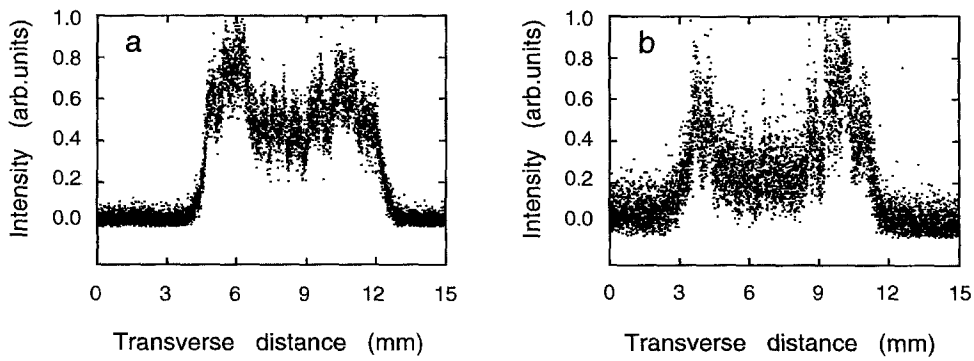

Fig. 4a, b. Spatial intensity distributions of the 6th-order AS pulse in n-H_2 (**a**) for the density of 3.3 amagat at 77 K and (**b**) for the density of 4.5 amagat at room temperature

Table 1. Comparison of the Raman gain coefficients

		n-H_2	p-H_2	n-D_2
77 K	Branch	$Q_{01}(1)$	$Q_{01}(0)$	$Q_{01}(2)$
	$\Delta N/N_0$ [a]	0.750	0.990	0.598
	$\Delta\nu/N_0$ [b]	42	29	39
	N_0	3.3	2.4	7.5
300 K	Branch	$Q_{01}(1)$	$Q_{01}(0)$	$Q_{01}(0)$
	$\Delta N/N_0$ [a]	0.660	0.510	0.385
	$\Delta\nu/N_0$ [b]	52	45	124
	N_0	4.5	–	8
Ratio of g_R at 77 K and g_R at 300 K		1.41	3.01	4.94

[a] ΔN denotes population difference between the initial and final states associated with Raman transitions; N_0 is the number density at the optimum operating condition

[b] $\Delta\nu$ is the Raman linewidth per unit density (MHz/amagat)

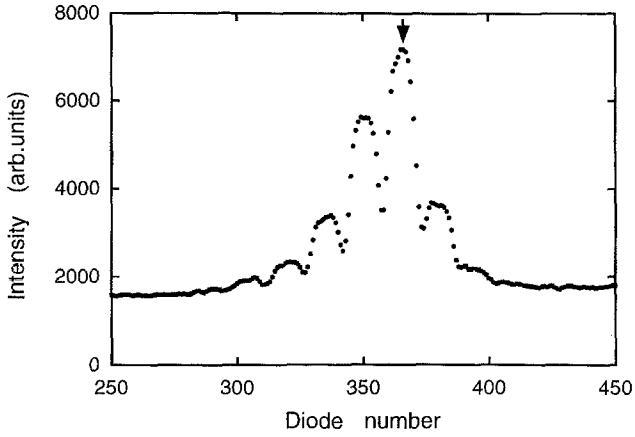

Fig. 6. Spectrum of the AS4 wave in p-H_2. The density was 2.3 amagat at 77 K. The *arrow* shows the center of the purely vibrationally scattered line of AS4 at 184.5 nm. Each subcomponent corresponds to the rotational shift of 354 cm^{-1}

amplitude of the ASn field is expressed as

$$\frac{dA_n}{dz} = \frac{\omega_n}{\omega_{-1}} \frac{g_R}{2} (A_0 A_{-1} A_{n-1} - A_{n-1}^2 A_n). \tag{2}$$

The first part on the right-hand side of (2) represents the four-wave Raman mixing contributing to the n-th anti-Stokes generation. The amplitude A_n increases in the phase-matching direction. The second part represents stimulated Raman scattering of ASn as a pump.

In the small-signal limit that $A_0(=P) \gg A_{-1}, A_{n-1}$, and A_n, we can neglect the second term in (2) and regard A_0 as constant. Equation (2) can be solved for A_1 to give

$$A_1 = \alpha \frac{\omega_1}{\omega_{-1}} \frac{2}{P^0} e^{Gz}, \tag{3}$$

where $G = \frac{g_R}{2} I_0 = \frac{1}{2} \frac{g_R}{2} P^2$. Applying the calculation for higher-order waves, the amplitude of ASn can be obtained as

$$A_n = \alpha^n \frac{\prod_{k=1}^{n} \omega_k}{\omega_{-1}^n} \frac{2^n}{n! P^{n-1}} e^{nGz}. \tag{4}$$

Thus,

$$M_n = \frac{A_n(77\,\mathrm{K})}{A_n(300\,\mathrm{K})} = \beta^n, \tag{5}$$

where $\beta \equiv \exp(\frac{1}{2} \Delta g_R I_0 z)$ and $\Delta g_R = g_R$ (77 K) $- g_R$ (300 K). Therefore, we can write

$$M_n = \beta M_{n-1} = \ldots\ldots = \beta^{n-1} M_1; \tag{6}$$

M_n increases monotonically because β is larger than unity. Thus, higher-order AS scattering might be enhanced compared with lower-order AS scattering when the Raman gas is cooled. Although the model is too simple to discuss the intensity-variation dependence on AS orders, the cooling-enhancement factor $\beta_n = M_n/M_{n-1}$ was investigated to determine if it has a certain constant value. The results are that $\overline{\beta_n} = 1.20 \pm 0.37$ for orders $n = 1$ to $n = 9$ of n-H_2 and $\overline{\beta_n} = 1.18 \pm 0.33$ for orders $n = 1$ to $n = 10$ of n-D_2. In this model, the fact that the values of β_n are similar suggests that Δg_R values coincide for n-H_2 and n-D_2.

Contrary to the expectation resulting from the increase of gain, no enhanced output was obtained by using p-H_2 instead of n-H_2, as shown in Fig. 4. For p-H_2, it was found that each AS line spread to several rotational side bands as shown in Fig. 6. Such rotational Raman components would arise through the Raman mixing effect with purely rotational and vibrational–rotational transitions. Even with a linearly polarized pump beam, the ratio of which was measured to be 1000:1, the generation of such rotational side bands was not suppressed. Accordingly, p-H_2 was not adequate for VUV generation since increased gains for purely rotational Raman transitions degraded vibrational AS scattering for up-conversion.

4 Conclusion

Stable outputs of AS pulses in the VUV have been obtained with a liquid-nitrogen-cooled Raman cell. Deposition on the exit window surface crucially affected performance and long-term operation was accomplished by keeping the temperature of the exit window at 250 K. The enhancement by cooling was found to be more significant for higher-order lines and an enhancement by a factor of 10 was obtained for n-H_2.

Acknowledgement. The authors thank Dr. M. Takenaga for valuable discussion and advice.

References

1. R.L. Byer: IEEE J. QE-**6**, 732 (1976)
2. P. Rabinowitz, A. Stein, R. Brickman, A. Kaldor: Appl. Phys. Lett. **35**, 739 (1979)

3. K. Midoikawa, H. Tashiro, Y. Aoki, K. Ohashi, K. Nagasaka, K. Toyoda, S. Namba: J. Appl. Phys. **57**, 1504 (1985)
4. D. Brink, D. Proch: Opt. Lett. **7**, 494 (1982)
5. H.F. Döbele, M. Hörl, M. Röwekamp: Appl. Phys. B **42**, 67 (1987)
6. H. Wallmeier, H. Zacharias: Appl. Phys. B **45**, 263 (1988)
7. V. Schulz-von der Gathen, T. Bornemann, V. Kornas, H.F. Döbele: IEEE. J. QE-**26**, 739 (1990)
8. S. Wada, A. Kasai, H. Tashiro: Opt. Lett. **17**, 97 (1992)
9. H. Moriwaki, S. Wada, H. Tashiro, K. Toyoda, A. Kasai, A. Nakamura: J. Appl. Phys. **74**, 2175 (1993)
10. G.W. Faris, M.J. Dyer: J. Opt. Soc. Am. **10**, 2273 (1993)
11. M. Spaan, A. Goehlich, V. Schulz-von der Gathen, H.F. Döbele: Appl. Opt. **33**, 3865 (1994)
12. K.D. van den Hout, P.W. Hermans, E. Mazur, H.F.P. Knaap: Physica. A **104**, 509 (1980)
13. W.K. Bischel, M.J. Dyer: Phys. Rev. A **33**, 3113 (1986)
14. D.K. Veirs, G.M. Rosenblatt: J. Mol. Spectrosc. **121**, 401 (1987)